THE JOURNAL OF PHYSICAL CHEMISTRY C

Article

pubs.acs.org/JPCC

The Electrical Double Layer of Dicationic Ionic Liquids at Onion-like Carbon Surface

Song Li,[†] Katherine L. Van Aken,[‡] John K. McDonough,[‡] Guang Feng,*[,†,§,∥] Yury Gogotsi,[‡] and Peter T. Cummings[†]

[†]Department of Chemical and Biomolecular Engineering, Vanderbilt University, Nashville, Tennessee 37235, United States

[‡]Department of Materials Science and Engineering & A.J. Drexel Nanotechnology Institute, Drexel University, Philadelphia, Pennsylvania 19104, United States

[§]State Key Laboratory of Coal Combustion, Huazhong University of Science and Technology, Wuhan 430074, China

[∥]School of Energy and Power Engineering, Huazhong University of Science and Technology, Wuhan 430074, China

Supporting Information

ABSTRACT: The electrical double layer (EDL) structure formed by ions at a charged surface, which is the key to determining the performance of supercapacitors, has been extensively studied for many monocationic ionic liquids (MILs). However, it is not known what effect replacing MILs with dicationic ionic liquids (DILs) will have on the EDL structure. In this work, the interfacial structure and electrochemical performance of DILs $[C_n(mim)_2](BF_4)_2$ (n = 3, 6, 9) and $[C_6(mim)_2](Tf_2N)_2$ were investigated using classical molecular dynamics (MD) simulation for comparison with their monocationic counterparts. Different EDL structures formed by DILs and MILs near an onion-like carbon (OLC) electrode were observed. The interfacial orientation of the imidazolium plane in dications was verified to be similar to that of monocations. Moreover, the dissimilar sizes of the cation/anion and the specific ion adsorption on OLC were found to contribute to the distinctive shape of the differential capacitance−electric potential (C−V) curves, which were also dependent on the type of anions. Increased capacitance in BF_4-containing DILs was not observed in comparison with their counterpart MILs, whereas dicationic $[C_6(mim)_2](Tf_2N)_2$ yielded higher differential capacitance in contrast to monocationic $[C_6mim][Tf_2N]$, which was substantiated by cyclic voltammetry measurements as well. This work provides molecular insights into the EDL structure and C−V curves of imidazolium-based DILs in OLC-based supercapacitors.

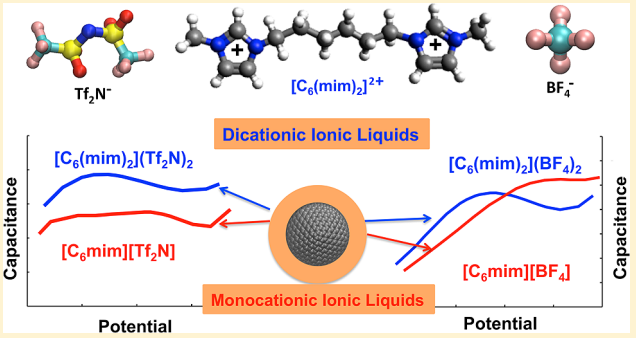

1. INTRODUCTION

Dicationic ionic liquids (DILs), consisting of two geminal cationic rings linked by alkyl chains at different lengths, can be used as catalysts,[1,2] solvents,[3] lubricants,[4] and electrolytes,[5,6] similar to applications for monocationic ionic liquids (MILs). An increasing number of studies on DILs have been recently reported. For instance, Anderson et al. have reported a series of DILs exhibiting high stability.[7] So far, the structural and dynamic properties of bulk DIL have been reported using molecular dynamics (MD) simulations.[8−11] However, the interfacial structure and the performance of DIL electrolytes in supercapacitors have yet to be investigated in detail. Since the structure and the molecular orientations of ions in electrical double layers (EDLs) at the surface of an electrode material play an important role in determining the energy stored in electric double layer capacitors (EDLCs),[12,13] it is of great interest to explore the role of DILs on their EDL structure and capacitive performance in contrast to that of MILs. Due to the more concentrated charge density of DILs as multivalent electrolytes compared with their monocationic counterparts, the performance of DILs is assumed to be quite different from MILs. In this work, the influences of alkyl chain length, ion size, and specific adsorption of DILs are investigated and compared with MILs.

The effects of the alkyl chain length of MILs on the capacitance of supercapacitors have been widely investigated using experimental[14−20] and computational techniques.[21,22] Fedorov et al. reported the transition of the differential capacitance−electric potential (C−V) curve from the bell to camel shape with the increase of the alkyl chain in MILs at the graphite electrode with a common anion using Monte Carlo simulation.[21] On the other hand, Vatamanu et al.'s MD simulation study[22] showed that the camel-shaped C−V curve obtained from planar graphite-based supercapacitors becomes less evident as the alkyl chain length increases, which is quasi-bell shaped. Although the C−V curve from experimental

Received: October 4, 2013
Revised: February 5, 2014

   dx.doi.org/10.1021/jp409888f | J. Phys. Chem. C XXXX, XXX, XXX−XXX

measurements varies depending on the electrode materials,[20] ion types,[20,23] temperature,[16,18,20] and ion size,[16,18,20] the overall differential capacitance is observed to decrease with the increase of the chain length due to the thicker EDL formed by cations with longer tails.[16,20] The transition in the shape of the C−V curve had not been reported experimentally until the recent study by Su et al., in which the transition of the bell- to camel-shaped C−V curves for Au(100)/imidazolium-based MILs was observed.[14] However, the effects of chain length on the C−V curve of carbon/DILs are still elusive. Thus, in this work, the imidazolium-based DILs with varying alkyl chain lengths are taken into consideration.

The relative size of the cation/anion also influences the shape of the C−V curves,[24,25] because the cation and anion dominate the EDL structure near negatively and positively charged electrodes, respectively.[12] The asymmetry of the C−V curve due to the dissimilar ion sizes was reported using mean field theory; i.e., smaller anions enhanced the capacitance at positive potential, and the increased capacitance at negative potential was observed for smaller cations.[25] Considering the asymmetric ion size of dications versus anions, the C−V curve for DILs is expected to be asymmetric as well. In addition, the C−V curve is also affected by the specific adsorption of ions on the electrode surface. It was reported that the adsorption of anions raises the capacitance at negative potential, whereas the capacitance is improved at positive potential by cation adsorption.[25] Therefore, the shape of the C−V curve is probably determined by the coeffect of ion size and specific adsorption.

In this work, molecular dynamics (MD) simulation was used to investigate the EDL structure of 1-alkyl-3-dimethylimidazolium tetrafluoroborate ($[C_n(mim)_2](BF_4)_2$, n = 3, 6, 9) and their C−V curves. Carbon nanomaterials are presently the most common electrode materials for EDLCs because of their high specific surface area and conductivity, low density, tunable surface chemistry, and electrochemical stability.[26−28] Onion-like carbon (OLC) was used as the electrode material in this study because of its high specific surface area and accessible surface stemming from its small particle size and exohedral structure,[29] which will help avoid mass transport effects found in nanoporous materials, especially at low temperature due to the high viscosity of electrolytes. To probe the influence of anion type on the C−V curve, the interfacial behavior and capacitive performance of $[C_6(mim)_2](Tf_2N)_2$ at an OLC surface were studied. The monocationic counterparts near the OLC surface were also explored for comparison with DILs.

2. METHODOLOGY

2.1. Simulation Setup. The simulation system consists of an OLC electrode immersed in a box of ionic liquids. The force field used for dications $[C_n(mim)_2]$ (n = 3, 6, 9) was adapted from the all-atom force field developed by Yeganegi et al.,[10] which has been validated to reproduce the experimental density with high accuracy. The force fields for monocations and anions were taken from the study of Lopes' group.[30] The van der Waals interaction parameters for carbon of the OLC electrode were taken from Cornell et al.'s study.[31] All the C−H bonds were constrained using the LINCS algorithm[32] during the simulation, and a 1.1-nm cutoff was used for van der Waals interactions. Long-range electrostatic interactions were processed using the particle mesh Ewald (PME) method.[33] Periodic boundary conditions (PBCs) were applied in three dimensions. All simulations were performed in a modified version of MD package Gromacs.[34] The OLC electrode with a radius of 1.22 nm was fixed in the center of a cubic box filled with ∼1000 ion pairs initially at low density. The equilibration was performed in the isobaric−isothermal ensemble at 1 bar and 800 K for 2 ns, followed by annealing the simulation to 450 K for $[C_n(mim)_2](BF_4)_2$ and 300 K for $[C_6(mim)_2](Tf_2N)_2$. The production runs were then conducted at 450 K in the NPT ensemble to ensure that $[C_n(mim)_2](BF_4)_2$ and $[C_6mim][BF_4]$ were in the liquid phase and the simulation was implemented at 300 K for $[C_6(mim)_2](Tf_2N)_2$ and $[C_6mim][Tf_2N]$ because of their low melting points. The time step of 1 fs was applied, and the trajectory was saved every 100 fs for computing the number and charge density profiles. The final box size is within 9−10 nm so that the ionic liquids far from the electrode surface exhibit bulk-like behavior. A 4-ns production run generated was used for further analysis. Different electric potentials were created by uniformly charging the electrode surface with varying charge densities, and the counterions were removed to ensure the neutrality of the simulation system (e.g., six dications were removed for an electrode surface charge density of +0.102 C/m^2). Although a different way to generate electric potential is applying a constant potential, it has been reported to result in almost the same electric double layer structure with the constant charge method, especially, within the potential range studied herein.[35] Since the results obtained in this work are based on the structure of EDLs, the constant charge method is still applicable here. The potential drop was calculated using Poisson's equation as in our previous studies.[36,37] A C−V curve is obtained by fitting the surface charge density as a function of electric potential using sixth order polynomials.

2.2. Materials and Experimental. OLC was synthesized by annealing of a nanodiamond precursor (UD90 grade, sp3 Technologies, USA) as described in our previous work.[38] Annealing was performed in a custom-made vacuum furnace (Solar Atmospheres, USA) at a temperature and pressure of 1800 °C and 10^{-6} Torr, respectively. The resultant structure is highly graphitic, and OLC can be considered as multilayered fullerenes with an ∼5−7 nm diameter.

The experimental tests were completed using rolled OLC films as electrodes and DIL $[C_6(mim)_2](Tf_2N)_2$ and MIL $[C_6mim][Tf_2N]$ as electrolytes in a typical supercapacitor device. The electrodes were made by mixing 95% OLC powder and 5% PTFE (60% in water, Aldrich, USA) binder, and the film was rolled to a thickness of 140 μm. The electrodes were punched to be 12 mm in diameter and then wetted with IL electrolytes before being placed into the Swagelok (USA) cell for testing. Two layers of PTFE separator (Gore, USA) were placed between the electrodes, and carbon coated aluminum disks were placed between the stainless steel Swagelok current collectors and the carbon electrode in order to minimize the interfacial resistance. When constructed, the Swagelok cells were kept under light pressure during testing to ensure good electrical contact between the components.

Cyclic voltammetry (CV) measured the current response of the device using a BioLogic VMP3 potentiostat/galvanostat (USA). The resulting current was normalized by the charge−discharge rate (0.5 mV/s), electrode mass, and surface area of the electrode (450 m^2/g) to display values in F/m^2.

3. RESULTS AND DISCUSSION

3.1. Interfacial Structure of DILs at OLC Surfaces. The number density profiles based on the center of mass of cations and anions, respectively, in DILs as a function of the distance

dx.doi.org/10.1021/jp409888f | J. Phys. Chem. C XXXX, XXX, XXX−XXX

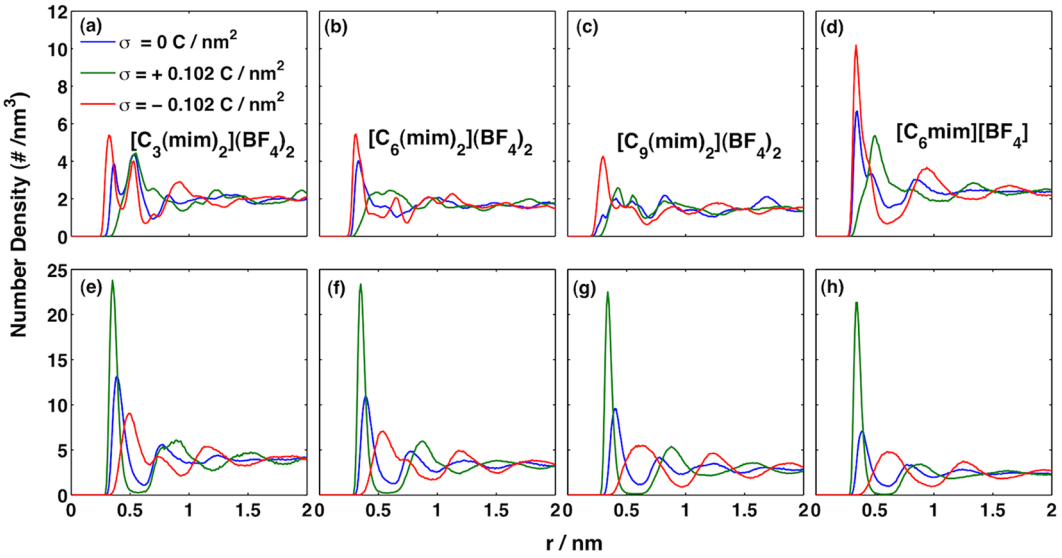

Figure 1. Number density profile for dicationic $[C_n(mim)_2](BF_4)_2$ (n = 3, 6, 9) and monocationic $[C_6mim][BF_4]$ ionic liquids at OLC surface, calculated from MD simulations. The top panels (a–d) are for cations and bottom panels (e–f) are for anions.

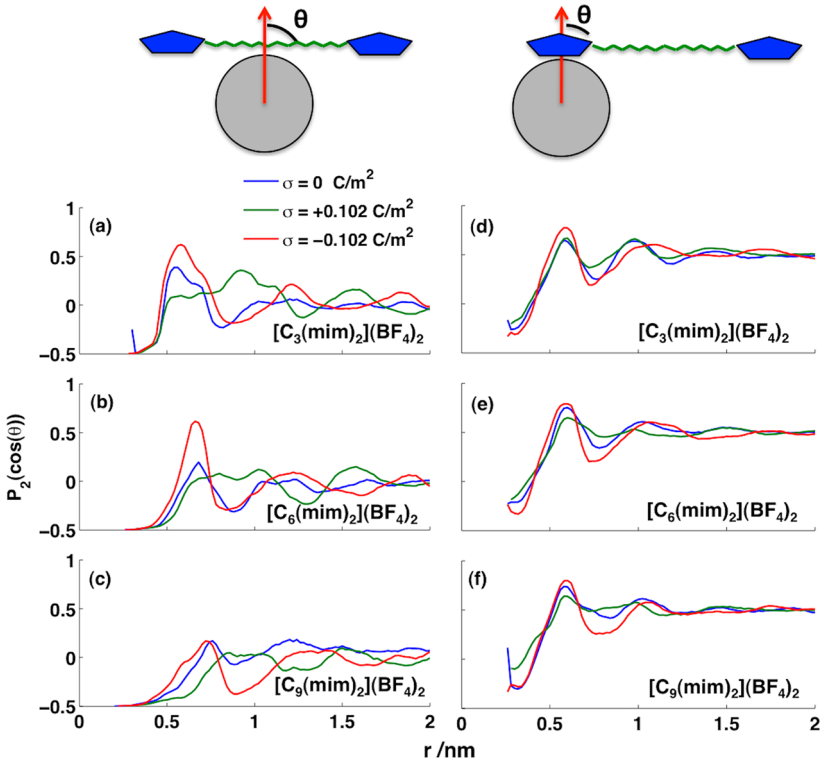

Figure 2. Orientational order parameter as a function of distance from OLC surface for the alkyl chain (a–c) and the imidazolium rings (d–f) in $[C_n(mim)_2](BF_4)_2$ (n = 3, 6, 9). The left panels (a–c) are for angles formed between the linkage alkyl chain in DILs and the normal to the OLC surface; the right panels (d–f) are for angles between the plane of the imidazolium ring and the normal to the OLC surface.

from the charged/uncharged OLC surfaces are presented in Figure 1. Layering of cations and anions near the OLC surface is present for both dicationic $[C_n(mim)_2](BF_4)_2$ (n = 3, 6, 9) and monocationic $[C_6mim][BF_4]$ regardless of the electrode's charge. In contrast to monocationic $[C_6mim][BF_4]$ (Figure 1d, h), the cation number density of $[C_n(mim)_2](BF_4)_2$ in the layer closest to OLC is evidently lower. Due to the large size and more concentrated charge density of dications, fewer are accumulated on the OLC surface, which is sufficient to counterbalance the opposite charges on the electrode surface. Moreover, a cation layer with twin peaks is formed near the neutral OLC surface for $[C_3(mim)_2](BF_4)_2$, whereas predominantly one dense layer of cations is observed for $[C_6(mim)_2](BF_4)_2$, $[C_9(mim)_2](BF_4)_2$, and monocationic $[C_6mim][BF_4]$. With the increase of the chain length, fewer cations are observed in EDLs, which is due to the decreased packing efficiency of the bigger dications. Because of the more concentrated charge density in dications, more anions in DILs are accumulated in the layer near OLC surfaces. A similar phenomenon is observed for $[C_6(mim)_2](Tf_2N)_2$ versus

dx.doi.org/10.1021/jp409888f | J. Phys. Chem. C XXXX, XXX, XXX–XXX

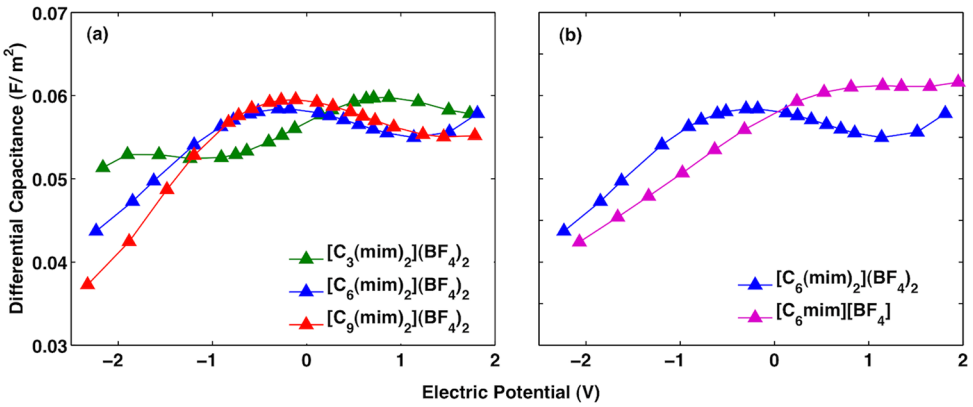

Figure 3. Differential capacitance−electrical potential (C−V) curves for $[C_n(mim)_2](BF_4)_2$ (n = 3, 6, 9) (a) and dicationic $[C_6(mim)_2](BF_4)_2$ versus monocationic $[C_6mim][BF_4]$ (b) from MD simulation.

$[C_6mim][Tf_2N]$ shown in Figure S1 of the Supporting Information (SI). Such a trend is consistent with that reported in MILs.[39,40] For charged electrodes, the number of counterions in EDLs increases as the chain length decreases.

To disclose more details of the interfacial structure of dications near the OLC surface, the orientational order parameter of dications near charged/uncharged OLC surfaces was calculated using $\langle P_2 \rangle = (3\cos^2(\theta) - 1)/2$ as shown in Figure 2. The orientational order parameter describes the distribution of angles formed by the cation chain or cation ring versus OLC surface (see cartoons in Figure 2). To describe the orientation of the cation chain, the angle was defined as angles formed by the linkage alkyl chain in DILs and the normal of the OLC surface. As shown in Figure 2a−c, the results suggested that the alkyl chains of cations in the first layer adsorbed on the OLC electrode tend to be parallel with the electrode surface regardless of the chain length or surface charge density, whereas those in the second layer tend to be perpendicular to the electrode surface. The latter is enhanced with the increase in negative charge density of the electrode except for $[C_9(mim)_2]^{2+}$. The longer alkyl chain in $[C_9(mim)_2]^{2+}$ with high flexibility may result in the more random arrangements relative to the electrode surface. For the cations beyond the second layer, there is no obvious orientational preference observed for the alkyl chains, consistent with observation of MILs.[40] To show how the cation ring is oriented, the angle defined is between the plane of the cation ring and the normal to the OLC surface. As shown in Figure 2d−f, at the OLC surface, the imidazolium plane tends to be parallel with the OLC surface, which facilitates the efficient packing of dications for better screening of the charged electrode. Meanwhile, the tendency of the vertical imidazolium plane in the second layer of EDLs is inspected. These observations imply that the imidazolium rings of DILs adopt the similar orientation near the carbon surface as reported for those in MILs.[39,41]

3.2. Capacitive Performance of $[C_n(mim)_2](BF_4)_2$. The C−V curves near OLC electrodes for DILs $[C_n(mim)_2](BF_4)_2$ (n = 3, 6, 9) with varying linkage chain lengths are shown in Figure 3a, and their corresponding surface charge densities versus electric potential are shown in Figure S2. The near-flat C−V curve featured OLC/RTIL supercapacitor has been reported in our previous studies.[36,37] However, in this work, differently shaped C−V curves were observed (Figure 3), where the differential capacitance at the negatively charged electrodes is higher than that at the positively charged electrodes. The shape of C−V curves is determined by multiple factors such as electrode materials, ion sizes, temperature, and different RTILs adopted.[36,37] In previous work, we chose RTILs (i.e., $[C_2mim][Tf_2N]$,[36] $[C_3mpy][Tf_2N]$,[37] $[C_4mpip][Tf_2N]$[37]) with cations and anions of similar sizes, which partially accounts for the near-flat C−V curve observed. In this study, the cation size is approximately 2−4 times that of the BF_4^- anion and the charge the cation carries is twice of that for the anion. This feature causes the favorable adsorbing and desorbing of more anions than cations in the EDL at the same potentials, since smaller anions can fit in a given volume.[42] Lauw et al. used mean field theory to demonstrate that, for RTILs with dissimilar cation/anion sizes, the shape of the C−V curve is dominated by the size of the counterions; i.e., the smaller counterion size leads to the enhanced differential capacitance.[25]

In addition, negative potential of zero charge (PZC) indicates the affinity of anions toward an electrode while positive PZC suggests preferential specific adsorption of cations.[25] The values of PZC for $[C_n(mim)_2](BF_4)_2$ are +0.10 V (n = 3), +0.18 V (n = 6), and +0.20 V (n = 9), and the PZC of $[C_6mim][BF_4]$ is +0.30 V. Based on these values, cations are preferred to be adsorbed on the OLC surface and the adsorption strength of dications increases with increasing chain length. Compared with dications, the adsorption of monocationic $[C_6mim]^+$ is favorable for OLC, and this adsorption of cations suggests the enhanced capacitance at positive potentials.[25] The combined effects of specific adsorption and ion size can well explain the shape of the C−V curves with higher capacitance at the positively charged electrode shown in Figure 3. Similarly, BF_4-containing MILs have been reported to exhibit asymmetric C−V curves as well, due to the dissimilar cation/anion sizes.[19,43−45]

The comparison of the C−V curves of dicationic $[C_6(mim)_2](BF_4)_2$ and monocationic $[C_6mim][BF_4]$ shown in Figure 3b highlights the slightly higher capacitance of $[C_6(mim)_2](BF_4)_2$ compared to $[C_6mim][BF_4]$ at negative potential and the reverse trend at positive potentials. However, Tf_2N-containing DILs display higher capacitance than MILs throughout the potential applied, which will be discussed later. The trends of C−V curves for BF_4-containing DILs and MILs suggest the better screening of anions in DILs than MILs at negative potentials and the more efficient screening of monocations than dications at positive potentials. In general, there is no significant enhancement of capacitance for DILs

dx.doi.org/10.1021/jp409888f | J. Phys. Chem. C XXXX, XXX, XXX−XXX

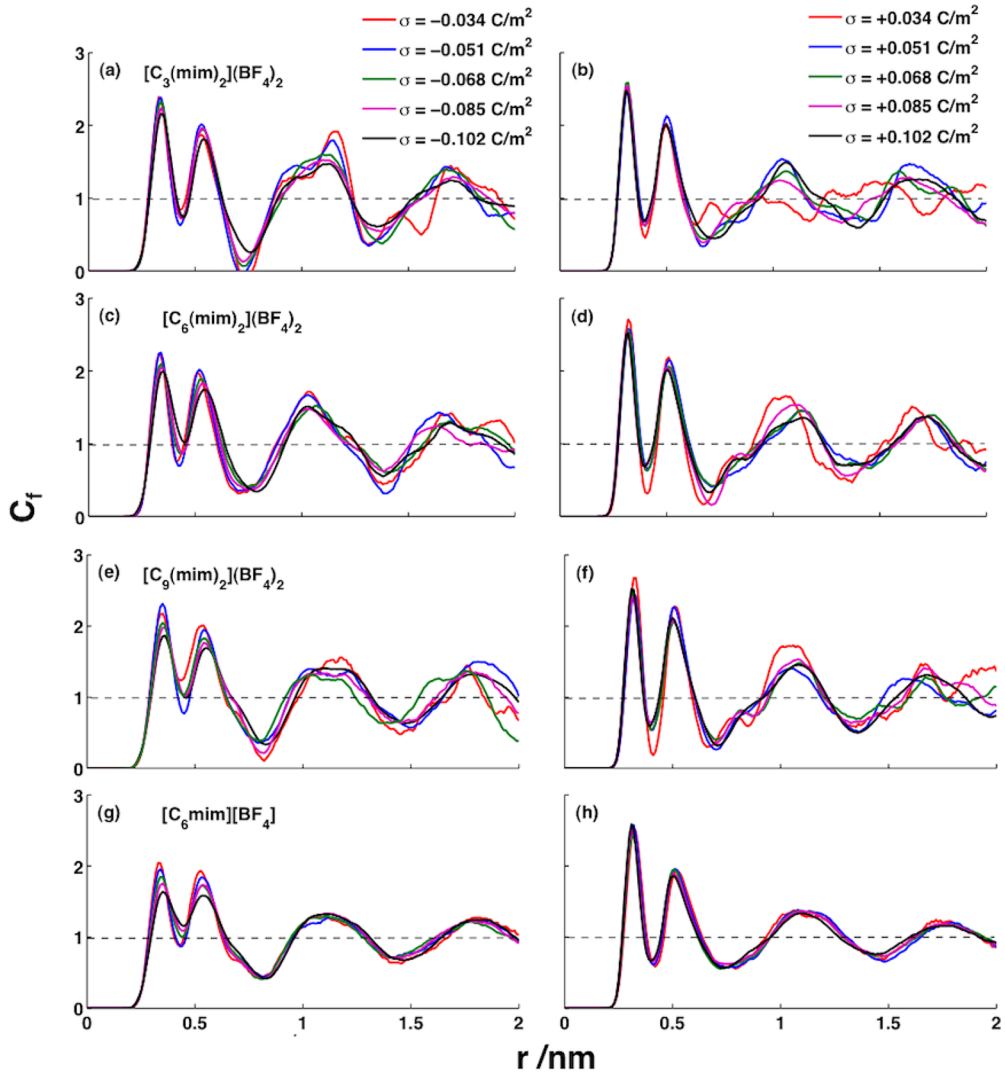

Figure 4. Charge screening factors for dicationic $[C_n(mim)_2](BF_4)_2$ (n = 3, 6, 9) and monocationic $[C_6mim][BF_4]$ at varying charge densities of electrode surface. The left panel is for the negatively charged electrode corresponding to an electric potential between −0.5 and −2.0 V, and the right panel is for the positively charged electrode at an electric potential between 0.5 and 2.0 V.

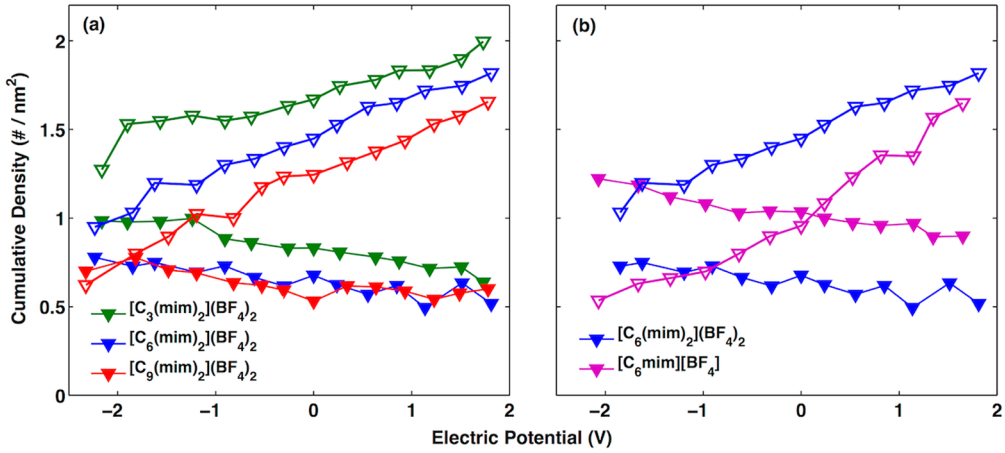

Figure 5. Cumulative density of ion's center-of-mass in the electric double layer as a function of electric potential applied from MD simulation for $[C_n(mim)_2](BF_4)_2$ (a) and $C_6(mim)_2](BF_4)_2$ versus monocationic $[C_6mim][BF_4]$ (b). The solid symbols denote cations, and hollow symbols are for anions.

compared with MILs, probably due to their similar screening efficiency, which is shown in Figure 4.

To evaluate the screening effects, a charge-screening factor is quantitatively defined by the equation below as[36]

dx.doi.org/10.1021/jp409888f | J. Phys. Chem. C XXXX, XXX, XXX−XXX

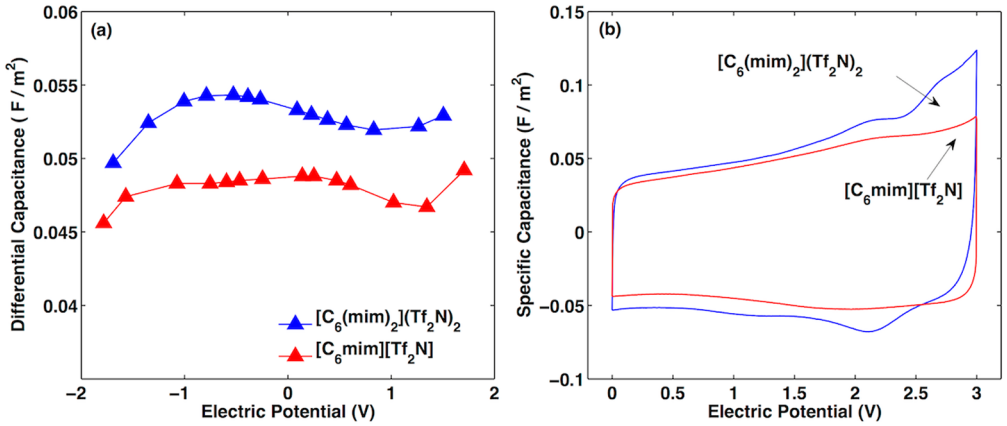

Figure 6. Differential capacitance as a function of electric potential obtained from MD simulation (a) and normalized cyclic voltammogram showing specific capacitance as a function of electric potential at a scan rate of 0.5 mV/s (b), for dicationic $[C_6(mim)_2](Tf_2N)_2$ and monocationic $[C_6mim][Tf_2N]$.

$$C_f(r) = -\int_R^r \frac{s^2}{R^2}\Delta\rho_e(s)\,\mathrm{d}s/\sigma$$

where s is the distance from the electrode, $\Delta\rho_e(s)$ is the change of charge density profile between the charged and neutral electrode, R is the radius of OLC, and σ is the electrode surface charge density. The charge screening factor for RTIL $[C_2mim][Tf_2N]$ is relatively constant with increasing surface charge density, and this factor was used to interpret the near-flat C−V curve for OLC-based supercapacitors in our previous work.[36] Herein, the calculated charge screening factors (C_f) for $[C_n(mim)_2](BF_4)_2$ at both positive and negative potentials are shown in Figure 4. The peak intensities in C_f decrease (longer chain, larger decrease) as the charge density/electric potential of the negative electrode increases, whereas a relatively insignificant variation in peak intensity is observed at the positive electrode. These trends agree with the decrease of differential capacitance (Figure 3) with increasing electric potential drop at negatively charged surfaces and the subtle variation in differential capacitance at positively charged surfaces. Such phenomena are related to the packing of counterions in EDLs near the OLC electrode. At a high potential on the negatively charged surface, the differential capacitance decreases with increasing chain length or cation size. This trend corresponds to the decreasing screening factors with the elongation of chain length (Figure 4). Moreover, the number of anions in EDLs near the positively charged electrode increases linearly with the surface charge density; therefore a near-constant screening factor was observed for the positively charged electrode. Conversely, for the negatively charged electrode, the number of cations does not increase linearly with the surface charge density, due to the complicated geometry, large size, and orientation of dications in EDLs. This observation is confirmed by examining the cumulative number density of ions, shown in Figure 5.

The cumulative number density of ions, i.e., the number of ions per unit area of electrode within the first layer (0−0.7 nm) of EDLs, was calculated as shown in Figure 5. The results indicate that more anions of $[C_n(mim)_2](BF_4)_2$ than cations were found to accumulate in EDLs near the positively charged electrodes, which contributes to the more efficient screening of smaller-sized anions. This is also reflected in the number density profile of Figure 1, which demonstrates that the anions are packed denser than the cations at either neutral or charged OLC surfaces. Moreover, the number of anions accumulated in EDLs exhibits a linear-like relationship with increasing electric potential at the positive electrodes, but not for cations at the negative electrodes, which is consistent with the variation in screening factors. On the other hand, the effect of the linkage chain length on the differential capacitance (i.e., in Figure 3a, the C−V curve for $[C_3(mim)_2](BF_4)_2$, $[C_6(mim)_2](BF_4)_2$, and $[C_9(mim)_2](BF_4)_2$) can be deduced from the cumulative number density. First, the bell-to-camel shape transition of the C−V curve is not observed with an increase in the linkage chain length. Compared with the MD simulation study by Vatamanu et al.,[22] however, the obtained C−V curves in Figure 3 cannot be classified into bell-, camel-, or U-shaped. The replacement of BF_4 anions used in this study with larger-sized anions may change the C−V curve shapes, and this was verified in the C−V curve of $[C_6(mim)_2](Tf_2N)_2$ (Figure 6a)

When the C−V curve of monocationic $[C_6mim][BF_4]$ was compared with that of dicationic $[C_6(mim)_2](BF_4)_2$, the higher anion density of EDLs in DILs compared to that of MILs, shown in Figure 5b, causes a more efficient screening by the positively charged electrode. The cumulative number densities of $[C_6(mim)_2](BF_4)_2$ and $[C_6mim][BF_4]$ at varying potentials indicate that more anions of $[C_6(mim)_2](BF_4)_2$ are adsorbed in EDLs compared to those in monocationic $[C_6mim][BF_4]$, which is also the case for $[C_6(mim)_2](Tf_2N)_2$ and $[C_6mim][Tf_2N]$ as shown in Figure S5. For the cumulative number density of cations, although a smaller amount of dication $[C_6(mim)_2]^{2+}$ is accumulated in EDLs, there is a higher concentration of positive charges in EDLs of $[C_6(mim)_2](BF_4)_2$ than in monocationic $[C_6mim][BF_4]$. From Figure 5, it is concluded that anions accumulate more rapidly than cations with increasing electric potential, which results in a higher differential capacitance at the positively charged electrode than at the negatively charged one.

3.3. C−V curves of $[C_6(mim)_2](Tf_2N)_2$ versus $[C_6mim][Tf_2N]$. To investigate the role of anions in EDLs, we replaced the anion of BF_4^- with Tf_2N^- and observed a different collection of C−V curves, as shown in Figure 6. Compared with MIL $[C_6mim][BF_4]$, a relative flatter C−V curve is observed in $[C_6mim][Tf_2N]$, which is also similar to previous studies[36,37] and explained by the relatively constant screening factors at both positively and negatively charged electrodes (Figure S6). Moreover, like $[C_n(mim)_2](BF_4)_2$, differential capacitance decays at high negative potential for $[C_6(mim)_2](Tf_2N)_2$.

dx.doi.org/10.1021/jp409888f | J. Phys. Chem. C XXXX, XXX, XXX−XXX

Lauw et al.'s mean field theory has demonstrated that not only ion size but also specific adsorption contributes to the asymmetry of the C−V curve; smaller anions raise the capacitance at positive potential and the specific adsorption of anions increases the capacitance at −1.2 to −0.3 V for ILs with cations and anions of equal size.[20,25]

As discussed above, the affinity of the ions toward the electrode also plays a role.[25] The values of PZC for $[C_6(mim)_2](Tf_2N)_2$ and $[C_6mim][Tf_2N]$ are −0.2 and −0.1 V, respectively. This indicates that Tf_2N^- is preferentially adsorbed on the OLC surface and the adsorption strength of cations on the OLC surface is in the order: C_6mim^+ > $C_6(mim)_2^+$. Combining the ion size effect and specific adsorption in the case of $[C_n(mim)_2](BF_4)_2$, both the smaller size of anions and the stronger specific adsorption of cations enhance the capacitance at positive potentials. In Tf_2N-containing ILs, the Tf_2N^- anion, which is larger than BF_4^-, reduces the capacitance at positive potentials, and the strong adsorption of Tf_2N^- raises the capacitance at negative potentials, thus yielding the near-flat C−V. Additionally, the size ratios of $C_6(mim)_2^+$:Tf_2N^- and C_6mim+:Tf_2N^- are 7:4 and 5:4, respectively, while the PZCs are −0.2 V and −0.1 V respectively. As a result, both the ion size and specific adsorption effects are more evident in dicationic $[C_6(mim)_2](Tf_2N)_2$ than monocationic $[C_6mim][Tf_2N]$. It is noteworthy that multiple factors may influence the shape of C−V curves aside from ion size and specific adsorption; therefore the C−V curve may be IL-specific depending on the ion chemistry, ion shape, orientation, and affinity toward the electrode.[20,23,46]

On average, dicationic $[C_6(mim)_2](Tf_2N)_2$ exhibits higher differential capacitance than monocationic $[C_6mim][Tf_2N]$ (−2.0 V to 2.0 V), which is not the fact for BF_4-containing DILs and MILs. The screening factors in Figure S6 displayed higher screening factors of $[C_6(mim)_2](Tf_2N)_2$ at both positive and negative potentials than those of $[C_6mim][Tf_2N]$, which could probably explain the observed different trends of capacitance between DILs and MILs with Tf_2N^- and BF_4^- as anions.

The enhanced capacitance in $[C_6(mim)_2](Tf_2N)_2$ is also verified experimentally by cyclic voltammetry shown in Figure 6b. However, this trend is only observed experimentally for cyclic voltammogram curves under a scan rate of 0.5 mV/s (synonymous with charge−discharge rate), since MD simulations were performed at the equilibrium state, which is close to the measurement at a very low scan rate. At a high scan rate (e.g., 50 mV/s), monocationic $[C_6mim][Tf_2N]$ displays a higher capacitance than $[C_6(mim)_2](Tf_2N)_2$ as shown in Figure S7. The accumulation of counterions in EDLs is a kinetic process: the faster motion of small ions counterbalances the electrode surface charges (the charging/discharging) within shorter times, whereas, for larger ions, the slower kinetics do not quickly balance the electrode surface charge, resulting in a lower capacitance.[47] At low scan rates, there is sufficient time for both large and small ions to accumulate in EDLs; i.e., both the electrode surfaces are well balanced by counter-charges, leading to DILs with higher packing density and screening efficiency exhibiting a higher capacitance.

4. CONCLUSION

In this study, the interfacial structure and the capacitive performance of DILs $[C_n(mim)_2](BF_4)_2$ with varying chain lengths and $[C_6(mim)_2](Tf_2N)_2$ near the OLC electrodes are investigated for the first time using MD simulations. The distinct interfacial structure of DILs was observed in comparison with their monocationic counterparts. Higher concentrations of DIL anions are found near the OLC surface regardless of the electrode's charge since each dication needs charge balance by two anions. The orientation of the dication near an OLC surface is similar to that of MILs. Moreover, regarding the capacitive performance of $[C_n(mim)_2](BF_4)_2$, the average capacitance at positively charged potential is higher than that at the negatively charged electrode, which is mostly attributed to the larger size of the dications compared to the BF_4^- anions. At negatively charged electrodes, the differential capacitance decreases with increasing chain length. It is also found that fewer counterions accumulate in EDLs for long-chain DILs based on the cumulative number density profiles. The C−V curve is substantiated to correspond to the variation of charge screening factors as a function of surface charge densities.

A near-flat C−V curve was observed for $[C_6mim][Tf_2N]$ as reported in previous studies[36,37] and attributed to the nearly constant charge screening factors with the variation of charge screening density. Both ion size and specific adsorption may influence the shape of C−V curves. The increased capacitance in $[C_6(mim)_2](Tf_2N)_2$ compared with $[C_6mim][Tf_2N]$ was observed via both MD and cyclic voltammetry and is due to the more efficient screening of electrode surface charges. Such enhancement was only found at low scan rates because of the different dynamics for small-sized monocations and large-sized dications; the slower motion of dications requires a longer time to balance the charges on the electrode surfaces. Since the use of DIL electrolytes in supercapacitors is impeded by their slow kinetic characteristics, in order to facilitate the use of DIL electrolytes in supercapacitors without compromising the power density, organic solvents such as propylene carbonate and acetonitrile were adopted to enhance the conductivity and charge/discharge rate.[6] However, the mechanism of the enhanced performance of DIL-based supercapacitors due to organic solvents is yet to be investigated, which will be addressed in our future work.

■ ASSOCIATED CONTENT

Supporting Information

Figures showing number density profile, electrode surface charge density versus electric potential, orientational order parameter, cumulative number density in EDL, charge screening factor and cyclic voltammogram at the scan rate 50 mV/s for $[C_6(mim)_2](Tf_2N)_2$ and $[C_6mim][Tf_2N]$. This information is available free of charge via the Internet at http://pubs.acs.org.

■ AUTHOR INFORMATION

Corresponding Author

*Telephone: 1-615-8754082. E-mail: guang.feng@vanderbilt.edu.

Notes

The authors declare no competing financial interest.

■ ACKNOWLEDGMENTS

This work was supported as part of the Fluid Interface Reactions, Structures, and Transport (FIRST) Center, an Energy Frontier Research Center funded by the U.S. Department of Energy, Office of Science, Office of Basic Energy Sciences. We acknowledge the National Energy

Research Scientific Computing Center, which is supported by the Office of Science of the U.S. Department of Energy under Contract No. DE-AC02-05CH11231. G.F. also appreciates the Palmetto cluster at Clemson University for providing computing resources. We thank Dr. Sheng Dai and Dr. Pasquale F. Fulvio (Oak Ridge National Laboratory) for providing ILs used in experiment.

REFERENCES

(1) Chinnappan, A.; Kim, H. Environmentally Benign Catalyst: Synthesis, Characterization, and Properties of Pyridinium Dicationic Molten Salts (Ionic Liquids) and Use of Application in Esterification. *Chem. Eng. J.* **2012**, *187*, 283−288.
(2) Fang, D.; Yang, J. M.; Jiao, C. M. Dicationic Ionic Liquids as Environmentally Benign Catalysts for Biodiesel Synthesis. *ACS Catal.* **2011**, *1*, 42−47.
(3) Han, X. X.; Armstrong, D. W. Using Geminal Dicationic Ionic Liquids as Solvents for High-Temperature Organic Reactions. *Org. Lett.* **2005**, *7*, 4205−4208.
(4) Pagano, F.; Gabler, C.; Zare, P.; Mahrova, M.; Dorr, N.; Bayon, R.; Fernandez, X.; Binder, W. H.; Hernaiz, M.; Tojo, E.; Igartua, A. Dicationic Ionic Liquids as Lubricants. *P. I. Mech. Eng. J.-J. Eng.* **2012**, *226*, 952−964.
(5) Zhancy, Z. X.; Zhou, H.; Yang, L.; Tachibana, K.; Kamijima, K.; Xu, J. Asymmetrical Dicationic Ionic Liquids Based on Both Imidazolium and Aliphatic Ammonium as Potential Electrolyte Additives Applied to Lithium Secondary Batteries. *Electrochim. Acta* **2008**, *53*, 4833−4838.
(6) Cho, W. J.; Yeom, C. G.; Kim, B. C.; Kim, K. M.; Ko, J. M.; Yu, K. H. Supercapacitive Properties of Activated Carbon Electrode in Organic Electrolytes Containing Single- and Double-Cationic Liquid Salts. *Electrochim. Acta* **2013**, *89*, 807−813.
(7) Anderson, J. L.; Ding, R. F.; Ellern, A.; Armstrong, D. W. Structure and Properties of High Stability Geminal Dicationic Ionic Liquids. *J. Am. Chem. Soc.* **2005**, *127*, 593−604.
(8) Li, S.; Feng, G.; Banuelos, J. L.; Rother, G.; Fulvio, P. F.; Dai, S.; Cummings, P. T. Distinctive Nanoscale Organization of Dicationic versus Monocationic Ionic Liquids. *J. Phys. Chem. C* **2013**, *117*, 18251−18257.
(9) Ishida, T.; Shirota, H. Dicationic versus Monocationic Ionic Liquids: Distinctive Ionic Dynamics and Dynamical Heterogeneity. *J. Phys. Chem. B* **2013**, *117*, 1136−1150.
(10) Yeganegi, S.; Soltanabadi, A.; Farmanzadeh, D. Molecular Dynamic Simulation of Dicationic Ionic Liquids: Effects of Anions and Alkyl Chain Length on Liquid Structure and Diffusion. *J. Phys. Chem. B* **2012**, *116*, 11517−11526.
(11) Bodo, E.; Chiricotto, M.; Caminiti, R. Structure of Geminal Imidazolium Bis(trifluoromethylsulfonyl)imide Dicationic Ionic Liquids: A Theoretical Study of the Liquid Phase. *J. Phys. Chem. B* **2011**, *115*, 14341−14347.
(12) Feng, G.; Zhang, J. S.; Qiao, R. Microstructure and Capacitance of the Electrical Double Layers at the Interface of Ionic Liquids and Planar Electrodes. *J. Phys. Chem. C* **2009**, *113*, 4549−4559.
(13) Fedorov, M. V.; Kornyshev, A. A. Towards Understanding the Structure and Capacitance of Electrical Double Layer in Ionic Liquids. *Electrochim. Acta* **2008**, *53*, 6835−6840.
(14) Su, Y. Z.; Yan, J. W.; Li, M. G.; Zhang, M.; Mao, B. W. Electric Double Layer of Au(100)/Imidazolium-Based Ionic Liquids Interface: Effect of Cation Size. *J. Phys. Chem. C* **2013**, *117*, 205−212.
(15) Alam, M. T.; Masud, J.; Islam, M. M.; Okajima, T.; Ohsaka, T. Differential Capacitance at Au(111) in 1-Alkyl-3-Methylimidazolium Tetrafluoroborate Based Room-Temperature Ionic Liquids. *J. Phys. Chem. C* **2011**, *115*, 19797−19804.
(16) Lockett, V.; Sedev, R.; Ralston, J.; Horne, M.; Rodopoulos, T. Differential Capacitance of the Electrical Double Layer in Imidazolium-Based Ionic Liquids: Influence of Potential, Cation Size, and Temperature. *J. Phys. Chem. C* **2008**, *112*, 7486−7495.
(17) Mayrand-Provencher, L.; Lin, S. X.; Lazzerini, D.; Rochefort, D. Pyridinium-Based Protic Ionic Liquids as Electrolytes for RuO2 Electrochemical Capacitors. *J. Power Sources* **2010**, *195*, 5114−5121.
(18) Costa, R.; Pereira, C. M.; Silva, F. Double Layer in Room Temperature Ionic Liquids: Influence of Temperature and Ionic Size on the Differential Capacitance and Electrocapillary Curves. *Phys. Chem. Chem. Phys.* **2010**, *12*, 11125−11132.
(19) Alam, M. T.; Islam, M. M.; Okajima, T.; Ohsaka, T. Measurements of Differential Capacitance at Mercury/Room-Temperature Ionic Liquids Interfaces. *J. Phys. Chem. C* **2007**, *111*, 18326−18333.
(20) Lockett, V.; Horne, M.; Sedev, R.; Rodopoulos, T.; Ralston, J. Differential Capacitance of the Double Layer at the Electrode/Ionic Liquids Interface. *Phys. Chem. Chem. Phys.* **2010**, *12*, 12499−12512.
(21) Fedorov, M. V.; Georgi, N.; Kornyshev, A. A. Double Layer in Ionic Liquids: The Nature of the Camel Shape of Capacitance. *Electrochem. Commun.* **2010**, *12*, 296−299.
(22) Vatamanu, J.; Borodin, O.; Bedrov, D.; Smith, G. D. Molecular Dynamics Simulation Study of the Interfacial Structure and Differential Capacitance of Alkylimidazolium Bis(trifluoromethanesulfonyl)-imide [$C_n$mim][TFSI] Ionic Liquids at Graphite Electrodes. *J. Phys. Chem. C* **2012**, *116*, 7940−7951.
(23) Kurig, H.; Vestli, M.; Tonurist, K.; Janes, A.; Lust, E. Influence of Room Temperature Ionic Liquid Anion Chemical Composition and Electrical Charge Delocalization on the Supercapacitor Properties. *J. Electrochem. Soc.* **2012**, *159*, A944−A951.
(24) Fedorov, M. V.; Kornyshev, A. A. Ionic Liquid near a Charged Wall: Structure and Capacitance of Electrical Double Layer. *J. Phys. Chem. B* **2008**, *112*, 11868−11872.
(25) Lauw, Y.; Horne, M. D.; Rodopoulos, T.; Nelson, A.; Leermakers, F. A. M. Electrical Double-Layer Capacitance in Room Temperature Ionic Liquids: Ion-Size and Specific Adsorption Effects. *J. Phys. Chem. B* **2010**, *114*, 11149−11154.
(26) Simon, P.; Gogotsi, Y. Capacitive Energy Storage in Nanostructured Carbon-Electrolyte Systems. *Acc. Chem. Res.* **2013**, *46*, 1094−1103.
(27) Simon, P.; Gogotsi, Y. Charge Storage Mechanism in Nanoporous Carbons and Its Consequence for Electrical Double Layer Capacitors. *Philos. Trans. R. Soc. London, Ser. A* **2010**, *368*, 3457−3467.
(28) Zhang, L. L.; Zhao, X. S. Carbon-Based Materials as Supercapacitor Electrodes. *Chem. Soc. Rev.* **2009**, *38*, 2520−2531.
(29) McDonough, J. K.; Gogotsi, Y. Carbon Onions: Synthesis and Electrochemical Applications. *Electrochem. Soc. Interface* **2013**, *22*, 61−66.
(30) Lopes, J. N. C.; Deschamps, J.; Padua, A. A. H. Modeling Ionic Liquids Using a Systematic All-Atom Force Field. *J. Phys. Chem. B* **2004**, *108*, 2038−2047.
(31) Cornell, W. D.; Cieplak, P.; Bayly, C. I.; Gould, I. R.; Merz, K. M.; Ferguson, D. M.; Spellmeyer, D. C.; Fox, T.; Caldwell, J. W.; Kollman, P. A. A Second Generation Force Field for the Simulation of Proteins, Nucleic Acids, and Organic Molecules. *J. Am. Chem. Soc.* **1995**, *117*, 5179−5197.
(32) Hess, B.; Bekker, H.; Berendsen, H. J. C.; Fraaije, J. G. E. M. Lincs: A Linear Constraint Solver for Molecular Simulations. *J. Comput. Chem.* **1997**, *18*, 1463−1472.
(33) Essmann, U.; Perera, L.; Berkowitz, M. L.; Darden, T.; Lee, H.; Pedersen, L. G. A Smooth Particle Mesh Ewald Method. *J. Chem. Phys.* **1995**, *103*, 8577−8593.
(34) Berendsen, H. J. C.; Vanderspoel, D.; Vandrunen, R. Gromacs - a Message-Passing Parallel Molecular-Dynamics Implementation. *Comput. Phys. Commun.* **1995**, *91*, 43−56.
(35) Merlet, C.; Pean, C.; Rotenberg, B.; Madden, P. A.; Simon, P.; Salanne, M. Simulating Supercapacitors: Can We Model Electrodes as Constant Charge Surfaces? *J. Phys. Chem. Lett.* **2013**, *4*, 264−268.
(36) Feng, G.; Jiang, D. E.; Cummings, P. T. Curvature Effect on the Capacitance of Electric Double Layers at Ionic Liquid/Onion-Like Carbon Interfaces. *J. Chem. Theory Comput.* **2012**, *8*, 1058−1063.

(37) Li, S.; Feng, G.; Fulvio, P. F.; Hillesheim, P. C.; Liao, C.; Dai, S.; Cummings, P. T. Molecular Dynamics Simulation Study of the Capacitive Performance of a Binary Mixture of Ionic Liquids near an Onion-Like Carbon Electrode. *J. Phys. Chem. Lett.* **2012**, *3*, 2465−2469.
(38) McDonough, J. K.; Frolov, A. I.; Presser, V.; Niu, J. J.; Miller, C. H.; Ubieto, T.; Fedorov, M. V.; Gogotsi, Y. Influence of the Structure of Carbon Onions on Their Electrochemical Performance in Supercapacitor Electrodes. *Carbon* **2012**, *50*, 3298−3309.
(39) Dou, Q.; Sha, M. L.; Fu, H. Y.; Wu, G. Z. Molecular Dynamics Simulation of the Interfacial Structure of $[C_n mim][PF_6]$ Adsorbed on a Graphite Surface: Effects of Temperature and Alkyl Chain Length. *J. Phys: Condens. Matter* **2011**, *23*, 175001.
(40) Ghatee, M. H.; Zolghadr, A. R.; Moosavi, F.; Ansari, Y. Studies of Structural, Dynamical, and Interfacial Properties of 1-Alkyl-3-methylimidazolium Iodide Ionic Liquids by Molecular Dynamics Simulation. *J. Chem. Phys.* **2012**, *136*, 124706−124719.
(41) Romero, C.; Moore, H. J.; Lee, T. R.; Baldelli, S. Orientation of 1-Butyl-3-methylimidazolium Based Ionic Liquids at a Hydrophobic Quartz Interface Using Sum Frequency Generation Spectroscopy. *J. Phys. Chem. C* **2007**, *111*, 240−247.
(42) Vatamanu, J.; Borodin, O.; Smith, G. D. Molecular Simulations of the Electric Double Layer Structure, Differential Capacitance, and Charging Kinetics for N-Methyl-N-propylpyrrolidinium Bis(fluorosulfonyl)imide at Graphite Electrodes. *J. Phys. Chem. B* **2011**, *115*, 3073−3084.
(43) Islam, M. M.; Alam, M. T.; Ohsaka, T. Electrical Double-Layer Structure in Ionic Liquids: A Corroboration of the Theoretical Model by Experimental Results. *J. Phys. Chem. C* **2008**, *112*, 16568−16574.
(44) Alam, M. T.; Islam, M.; Okajima, T.; Ohsaka, T. Ionic Liquid Structure Dependent Electrical Double Layer at the Mercury Interface. *J. Phys. Chem. C* **2008**, *112*, 2601−2606.
(45) Alam, M. T.; Islam, M. M.; Okajima, T.; Ohsaka, T. Measurements of Differential Capacitance in Room Temperature Ionic Liquid at Mercury, Glassy Carbon and Gold Electrode Interfaces. *Electrochem. Commun.* **2007**, *9*, 2370−2374.
(46) Kurig, H.; Vestli, M.; Janes, A.; Lust, E. Electrical Double Layer Capacitors Based on Two 1-Ethyl-3-methylimidazolium Ionic Liquids with Different Anions. *Electrochem. Solid. St. Lett.* **2011**, *14*, A120−A122.
(47) Richey, F. W.; Dyatkin, B.; Gogotsi, Y.; Elabd, Y. A. Ion Dynamics in Porous Carbon Electrodes in Supercapacitors Using in Situ Infrared Spectroelectrochemistry. *J. Am. Chem. Soc.* **2013**, *135*, 12818−12826.